Biosensors and Bioelectronics 132 (2019) 1–7

Contents lists available at ScienceDirect

Biosensors and Bioelectronics

journal homepage: www.elsevier.com/locate/bios

Manganese doped CdS sensitized graphene/Cu_2MoS_4 composite for the photoelectrochemical immunoassay of cardiac troponin I

Huitong Chi[a,1], Qingzhi Han[a,1], Tianhe Chi[b], Bin Xing[a], Ning Ma[a], Dan Wu[a,*], Qin Wei[a]

[a] Key Laboratory of Interfacial Reaction & Sensing Analysis in Universities of Shandong, School of Chemistry and Chemical Engineering, University of Jinan, Jinan 250022, PR China

[b] Department of Cardiology, the Third People's Hospital of Liaocheng, Liaocheng 252000, PR China

ARTICLE INFO

Keywords:
Label-free immunosensor
Photoelectrochemistry
Cardiac troponin I
Mn doped CdS
G/Cu_2MoS_4@CdS:Mn composite

ABSTRACT

As a newly emerged photoactive material, Cu_2MoS_4 has motivated wide research interests in the field of photoelectrochemistry. Based on manganese doped CdS (CdS:Mn) sensitized graphene (G)/Cu_2MoS_4 composite, we developed a label-free photoelectrochemical (PEC) immunosensor for the detection of cardiac troponin I (cTnI). G as an excellent 2D conductive material, combined with Cu_2MoS_4 could improve its charge transfer efficiency. CdS:Mn nanoparticles (NPs) loaded on G/Cu_2MoS_4 further enlarged the light absorption range of Cu_2MoS_4 and restrained the electron-hole pairs recombination. Under optimal conditions, the proposed PEC immunosensor responded sensitively to cTnI with a low detection limit of 0.18 pg/mL and a wide linear range (0.005–1000 ng/mL). Moreover, as-fabricated immunosensor also exhibited high sensitivity, excellent selectivity and good stability. This work also was extended to real samples analysis and obtained satisfied results.

1. Introduction

Cardiovascular disease (CVD) is a common type of circulatory disease, the prevalence and mortality continue to rise (Kim and Sillah, 2013). The patients with myocardial injury generally have chronic or severe acute skeletal muscle injury (Adams et al., 1993). In order to improve the survival rate, CVD needs early diagnose. The biochemical markers of early myocardial injury are mainly limited to creatine phosphate kinase (CK) (Kucherenko et al., 2015), myoglobin (MB) (Qing et al., 2015), creatine kinase MB subform (CK-MB) (Mcdonnell et al., 2009) and cardiac troponin I (cTnI) (Shumkov et al., 2013; Zhang et al., 2018). However, CK, MB and CK-MB exist not only in myocardial tissue, but also in non-myocardial tissue. When skeletal muscle is damaged, they also increased in varying degrees. As for cTnI, not only it can reveal the tiny myocardial damage, but also can remain in myocardial tissue for a long time. Therefore, cTnI is an ideal biomarker of myocardial cell damage (acute coronary syndrome and acute myocardial infraction) (Falahati et al., 1999; Kim et al., 2016). For all the above reasons, a valid and sensitive method to diagnose CVD by detecting cTnI is reasonable.

Till now, various methods of detecting cTnI have been reported, such as electrochemical (Ahammad et al., 2011; Chekin et al., 2018; Ko et al., 2007), enzyme-linked immunosorbent assay (ELISA) (Asiabanha et al., 2016; Cummins and Cummins, 1987), radioimmunoassay (Cummins et al., 1987; Zhou et al., 2018), surface plasmon resonance (SPR) (Masson et al., 2004; Wu et al., 2017), electrochemiluminescence (Shen et al., 2011), etc. Compared with the above methods, photoelectrochemical (PEC) immunoassay as a new analytical method, is more convenient, economical and easier miniaturize (Haddour et al., 2006). PEC immunoassay has excellent combination of the immanent sensitivity of the PEC bioanalysis and the specific bioaffinity properties of the immunomolecules (Zhao et al., 2017). In the process of PEC detection, light energy is used to excite photoactive materials and current is used as the detection signal. This procedure is inverse of electrochemiluminescence (Wang et al., 2009b). PEC immunosensor is evolved from electrochemistry, because the total separation and the diverse energy form of the motivation source and detection signal, its sensitivity is more higher than the traditional methods (Fan et al., 2014b; Lv et al., 2017).

Recently, various semiconductor materials have been used to fabricate the PEC biosensors. Such as metal sulfide, including Bi_2S_3 (Sun et al., 2014), MoS_2 (Wang et al., 2017b), SnS_2 (Zhang et al., 2017b), $ZnIn_2S_4$ (Han et al., 2015), Cu_2MoS_4 and so on, get more and more attention. Among them, Cu_2MoS_4 as a representative ternary transition metal chalcogenide, is earth-enough, pollution-free and low-cost (Ma et al., 2017; Chen et al., 2014). Nevertheless, Cu_2MoS_4 has low

* Corresponding author.
E-mail address: wudan791108@163.com (D. Wu).
[1] These authors contributed equally to this work.

https://doi.org/10.1016/j.bios.2019.02.048
Received 5 December 2018; Received in revised form 7 February 2019; Accepted 18 February 2019
Available online 27 February 2019
0956-5663/

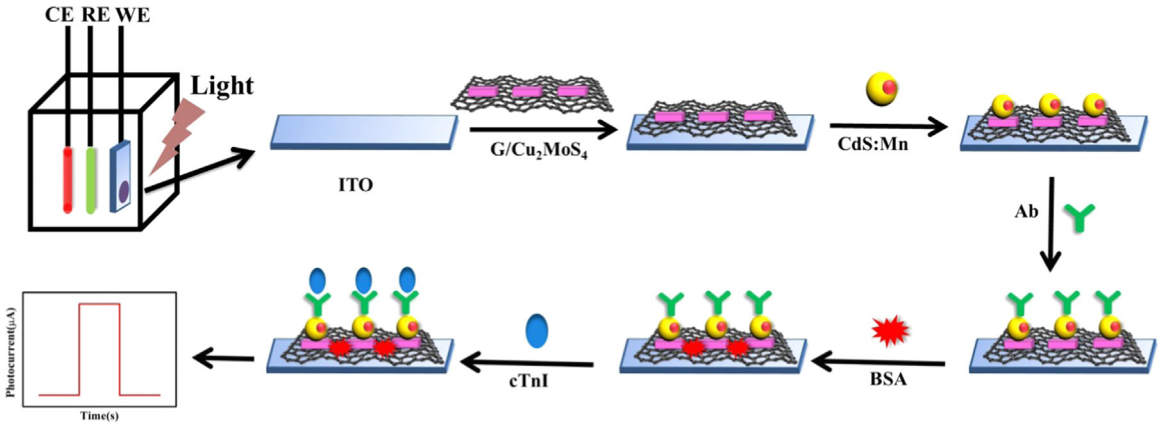

Schemee 1. Fabrication process of the proposed PEC biosensor.

photocurrent conversion efficiency and high electron hole recombination rate. In order to enhance the photocurrent intensity of Cu_2MoS_4, a narrow band gap material could be introduced as a sensitizer to enlarge its light absorption range. CdS is a narrowband gap semiconductor and often used to sensitize wide band gap semiconductors (Wang et al., 2016; Zhan et al., 2016). Because CdS could enhance the light energy utilization rate and promote the electron-hole separation efficiency. Furthermore, when Mn is doped in CdS, the light absorption ability of CdS could be further enhanced (Zhang et al., 2017a). Graphene (G) with the large superficial area and unexceptionable bonding performances, could be used to improve the electron transfer rate of semiconductors (Gopalan et al., 2016).

In this protocol, a novel label-free PEC immunosensor by using G/Cu_2MoS_4@CdS:Mn as a matrix to detect cTnI is developed. Scheme 1 illustrated the fabrication process of the PEC immunosensor. First, the Indium-Tin Oxides (ITO) electrode was modified with G/Cu_2MoS_4 composite, then the CdS:Mn nanoparticles (NPs) were added to form G/Cu_2MoS_4@CdS:Mn matrix for the immobilization of cTnI antibody (Ab). Next, the bovine serum albumin (BSA) was employed to block the nonspecific active sites of electrodes (Li et al., 2017a; Ren et al., 2017b). Then, the cTnI antigen (Ag) was bound to the electrode surface by the specific Ab-Ag reaction. Finally, a label-free PEC immunosensor for cTnI detection was finished.

2. Experimental section

2.1. Materials and reagents

Ascorbic acid (AA) and Chitosan (CS) were purchased from Sinopharm Chemical Reagent Co., Ltd (China). NaOH was obtained from Jinan reagent general plant. Manganese acetate ($Mn(Ac)_2{\cdot}4H_2O$) was obtained from Tianjin Kermel Chemical Co., Ltd. N-(3-Dimethylaminopropyl)-N-ethyl-carbodiimide hydrochloride (EDC) and N-hydroxy succinimide (NHS) were purchased from Shanghai Civi-Chem Co., Ltd. The phosphate buffer solution (PBS) was used in the whole experiment with pH = 7.4. All other chemical reagents were used without further treatment.

2.2. Apparatus

PEC tests were carried on a PEC workstation (Zahner Zennium PP211, Germany) with light excitation source which was purchased from Zahner (Germany). Other apparatus was provided in Supplementary information.

2.3. Preparation of the G/Cu_2MoS_4 complex solution

0.25 mg of G was added to 0.5 mL deionized water and ultrasonic for 2 h. Following, 0.5 mL 6 mg/mL of Cu_2MoS_4 (the preparation of Cu_2MoS_4 was given in Supporting information) was added and stirred for 5 h to disperse it evenly.

2.4. Construction process of ITO/G/Cu_2MoS_4 and ITO/G/Cu_2MoS_4@CdS:Mn electrodes

The ITO slices (20 × 7 mm^2) must be washed before use. The ITO slices was washed (under ultrasonic) with acetone, ethyl alcohol, 1 mol/L NaOH ethyl alcohol/ultrapure water mix solution (v/v = 1:1) and ultrapure water for 30 min separately, and then dried at 70 °C in nitrogen atmosphere for 140 min. In order to obtain the ITO/G/Cu_2MoS_4 electrodes, 10 μL of the above synthesized G/Cu_2MoS_4 suspensions were dropped onto ITO electrodes and dried in darkness.

CdS:Mn NPs loaded on G/Cu_2MoS_4 electrodes were through the successive ionic layer adsorption and reaction (SILAR) method and with some modifications (Fan et al., 2014a). Before the preparation of G/Cu_2MoS_4@CdS:Mn electrodes, 5 μL of CS (0.5 wt%) solution was dropped on the surface of G/Cu_2MoS_4 electrodes to form a film, which could enhance the adhesion force between semiconductor materials and ITO. Then, the G/Cu_2MoS_4 electrodes were successively immersed into 0.1 mol/L $Cd(NO_3)_2$ methanol solution (containing 0.08 mol/L $Mn(Ac)_2$), 0.1 mol/L Na_2S methanol/water mixture (v/v = 1:1) for 30 s, respectively. The electrodes were washed with methanol after each immersion. The SILAR cycle was repeated several times to modify CdS:Mn on G/Cu_2MoS_4 electrodes, and then the ITO/G/Cu_2MoS_4@CdS:Mn electrodes were obtained.

2.5. Construction of the immunosensor

First, as-fabricated ITO/G/Cu_2MoS_4@CdS:Mn electrodes were immersed in thioglycolic acid (TGA) aqueous solution (10 mmol/L) for 10 min to immobilize -COOH groups ($(CdS)^-$-S-CH_2-COOH) (Han et al., 2017) on its surface. Following the electrodes were rinsed with water to remove excess TGA. Next, 5 μL 0.4 mol/L EDC + 0.1 mol/L NHS mixed solution was added and stored in a 4 °C refrigerator for 1 h to activate -COOH groups, following washed with water as well (Han et al., 2017). Whereafter, 5 μL 10 μg/mL cTnI Ab was added onto the electrodes and incubated at 4 °C for 3 h, and then rinsed with water to remove physically combined Ab. Then, 5 μL 1% BSA (PBS solvent) was added to block nonspecific binding sites (Tong et al., 2018). After incubated at 4 °C for 3 h, the electrodes were rinsed with water thoroughly. After that, 5 μL different concentrations of cTnI Ag were dropped onto the electrodes and incubated at 4 °C for 2 h, then washed with water to remove nonspecific bonds. Finally, a label-free PEC immunosensor for cTnI detection was obtained.

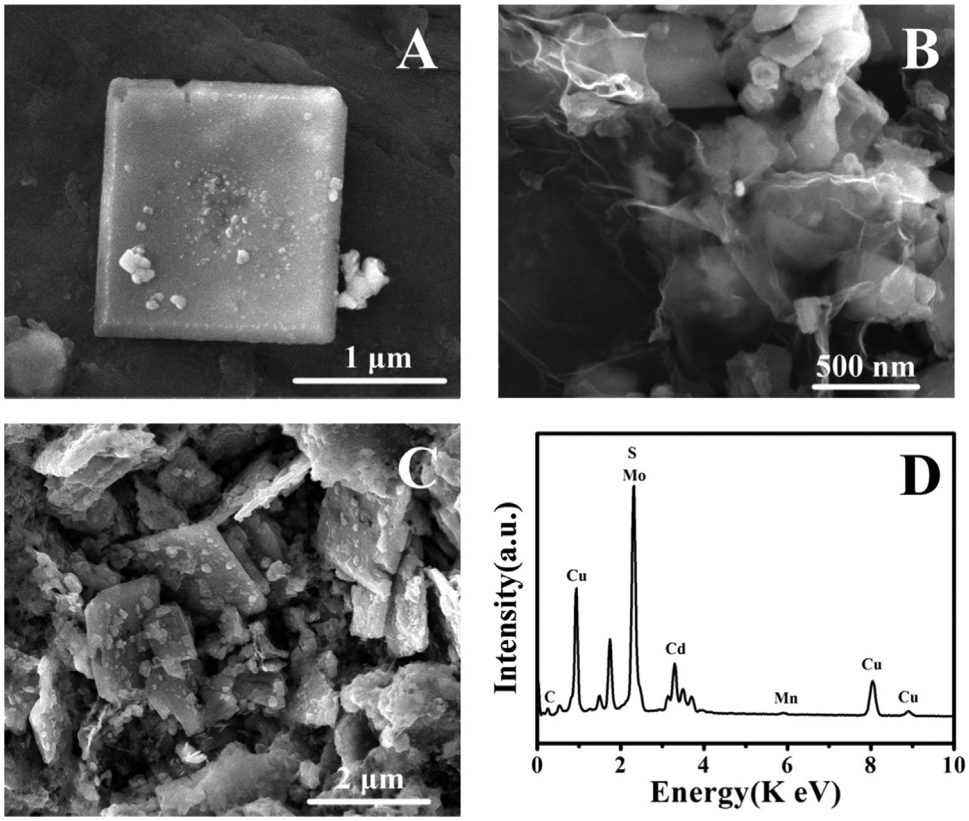

Fig. 1. SEM image of (A) Cu_2MoS_4, (B) G/Cu_2MoS_4 composite, (C) CdS:Mn modified G/Cu_2MoS_4 electrode and (D) EDS figure of the G/Cu_2MoS_4@CdS:Mn electrode.

2.6. PEC detection

PEC detection was carried out in PBS solution (containing 0.1 mol/L AA) on a PEC workstation (light intensity 180 $W{\cdot}m^{-2}$ with 0 V applied potential). A three-electrode system was used in the measurements, consisted of a Pt wire electrode (counter electrode, CE), a saturated calomel electrode (SCE reference electrode, RE) and a working electrode (ITO, WE).

3. Results and discussion

3.1. Characterization of the synthesized materials

Fig. 1 A shown the scanning electron microscopic (SEM) of Cu_2MoS_4. As can be seen from the picture, the Cu_2MoS_4 was a sheet-like structure and with a size of ~1.5 μm. In addition, Cu_2MoS_4 has a larger specific surface area which could load more CdS:Mn to increase the absorption of light energy. Fig. 1 B indicates that Cu_2MoS_4 was loaded at G by physical commixture to enhance conductivity. From Fig. 1 C we could see that CdS:Mn NPs loaded on G/Cu_2MoS_4 and formed the G/Cu_2MoS_4@CdS:Mn hybrid structure. As shown in Fig. S1 (Supporting information), the diameter of CdS:Mn NPs is about 11 nm and the lattice fringes are clear. As depicted in the energy dispersive spectrometer (EDS) spectrum (Fig. 1 D), the main component elements of G/Cu_2MoS_4@CdS:Mn specimen is Cu, Mo, S, C, Cd and Mn. The result of elemental mapping images (Fig. S2) agreed with the EDS spectrum, demonstrated the successfully synthesized of G/Cu_2MoS_4@CdS:Mn.

Furthermore, the high crystallinity and crystalline structure of the synthetic materials were verified by the X-ray power diffraction (XRD). Fig. 2 A (a) shows that the diffraction peaks matched well with the pure Cu_2MoS_4 (Chen et al., 2014). After Cu_2MoS_4 coupling with G, there was no other diffraction peaks appeared (Fig. 2 A (b)), indicating the G introduction did not change the phase structure of Cu_2MoS_4. And the diffraction peaks became weaken, the reason might be that Cu_2MoS_4 crystals were covered by G (Yan et al., 2016) and the crystallinity of composites were reduced (Si et al., 2018). As shown in Fig. 2 A (c), the diffraction peaks at 29.37°, 38.03°, 47.41° and 69.55° were corresponding to the crystal planes (111), (200), (220), and (400) of Mn doped CdS (JCPDS No. 21–0829). In order to further analyze the oxidation state of the synthesized Cu_2MoS_4, the X-ray photoelectron spectroscopy (XPS) spectrum (Fig. 2 B) of the specimen was also performed, and the detailed analyses were revealed in Fig. S3. In addition, the element oxidation state in CdS:Mn NPs was Cd^{2+}, S^{2-} and Mn^{2+}, respectively (Fan et al., 2014a; Sankapal et al., 2000; Santra and Kamat, 2012).

3.2. Characterization of the as-fabricated PEC immunosensor

In order to restrain the electron-hole recombination rate and promote electron-hole separation efficiency, AA (0.1 mol/L) was used as the electronic donor to capture the photogenerated hole of CdS:Mn. Each modification step could be monitored by the time-based photocurrent response (Fig. 3 A), and all the tests were carried out under the irradiation of 450 nm light. The bare ITO (Fig. 3 A; curve a) shows no photocurrent.

After the addition of Cu_2MoS_4 (curve b), the ITO/Cu_2MoS_4 electrode shows a bigger photocurrent than curve a. When Cu_2MoS_4 and G physically mixed (curve c), the photocurrent continuously increased, which could ascribe to the good electrical conductivity of G. After the CdS:Mn NPs (curve d) modified onto the surface of ITO/G/Cu_2MoS_4 by SILAR method, the photocurrent increased greatly (about 41.5 μA). This could be attributed to the fact that the CdS:Mn NPs enhanced the absorption of visible light and suppressed the recombination of electron-hole pairs. Next, the -COOH groups was added (via TGA CdS reaction) and activated by EDC/NHS. The obtained ITO/G/Cu_2MoS_4@CdS:Mn electrode was used as matrix for the following immobilization of Ab (curve e), BSA (curve f), and cTnI (curve g). The gradually reduced photocurrent could attribute to the modified protein (Ab, BSA, cTnI)

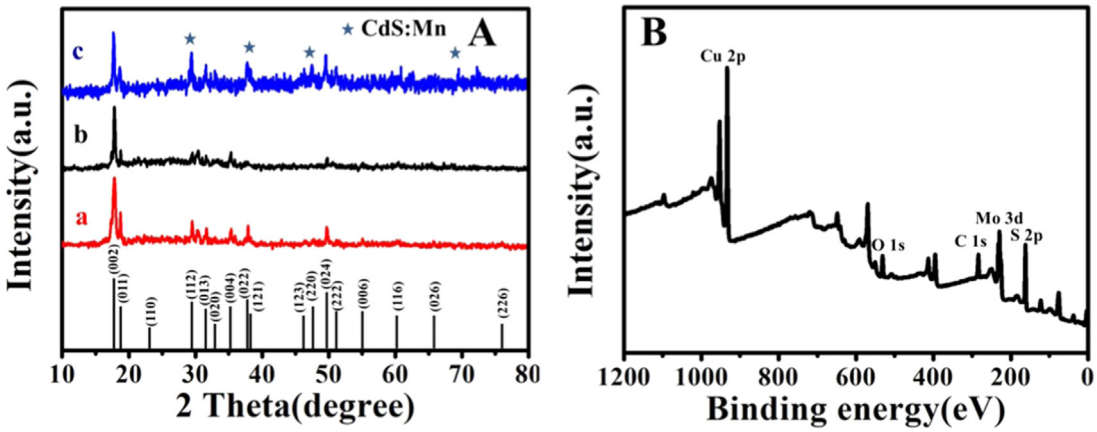

Fig. 2. (A) XRD patterns of (a) pure Cu_2MoS_4, (b) G/Cu_2MoS_4, (c) G/Cu_2MoS_4@CdS:Mn. (B) XPS survey spectra of the Cu_2MoS_4.

impeded the charge transfer and hindered the surface reaction between the electron donor and the photoinduced holes.

The Electrochemical impedance spectroscopy (EIS) is a powerful tool to monitor the electron transfer resistance, which can be used to demonstrate whether or not the PEC immunosensor was successfully fabricated. (Fan et al., 2016; Wu et al., 2016; Xing et al., 2018). In the EIS test, the counter electrode (Pt wire), reference electrode (SCE) and working electrode were immersed in a 5.0 mmol/L $[Fe(CN)_6]^{3-/4-}$ solution containing 0.1 mol/L KCl without irradiation and the applied frequency range of EIS spectra was 0.1–10^5 Hz. The Nyquist plot of different modified steps was shown in Fig. 3 B. From the picture we could see that the impedance spectrum is a semicircular at the higher frequency and straight at the lower frequency. In the picture, the semicircle part represents the charge transfer resistance (R_{et}, associated with the electrode surface change), and the linear part equals to the diffusion step throughout the process (Ren et al., 2017c). The upper inset of Fig. 3 B is the corresponding equivalent circuit, which consisted of electron transfer resistance (R_{et}), the solution resistance (R_s), the double layer capacitance (C_{dl}) and the Warburg impedance (Z_w). The lower inset of Fig. 3 B is the magnified image of curve (a), (b) and (c). It can be seen from Fig. 3 B (a), there is a very small semicircle diameter of the bare ITO electrode. After Cu_2MoS_4 (curve b) loaded on the surface of ITO electrodes, the semicircular diameter obviously increased, this could be attributed to the characteristic of the semiconductor materials. However, when the electrodes modified with the G/Cu_2MoS_4 (curve c) composites, the semicircular diameter reduced, this is because G improved its electron conduction ability. After the electrodes modified with chitosan (CS) (curve d), the semicircular diameter increased, which could be attributed to the insulation characteristic of CS (Wang et al., 2009a). The semicircular diameter slightly increased after CdS:Mn (curve e) loaded on the surface of ITO electrodes because of its semi-conduction. Following, with the modification of Ab (curve f), BSA (curve g), and cTnI (curve h), the resistance R_{et} continuously enhanced, which could be ascribed to the non-conductive feature of the proteins. All of the above results proved that each of the modification steps was successfully.

Scheme 2 illustrates the mechanism of electron-hole transfer of the proposed immunosensor. As shown in the scheme, when the CdS:Mn NPs absorbed photon energy is higher than its band gap, the electron could transfer from the valence band (VB) to the conduction band (CB). After CdS:Mn coupled with Cu_2MoS_4, the electron of CdS:Mn could be rapidly transferred to the CB of Cu_2MoS_4 and G, leaving the electrons to be collected by ITO glass as a photocurrent and the holes neutralized by the reductive AA.

3.3. Optimization of experimental conditions

In order to obtain the best performance of the as-fabricated PEC immunosensor, the experimental conditions need to be optimized (Ren et al., 2017a). The influences of different Cu_2MoS_4 concentrations are shown in Fig. S4 A. The photocurrent intensity increased with the concentration of Cu_2MoS_4 from 2.0 mg/mL to 3.0 mg/mL. However, with the concentration of Cu_2MoS_4 further increased, the photocurrent intensity decreased gradually. This phenomenon could be interpreted as

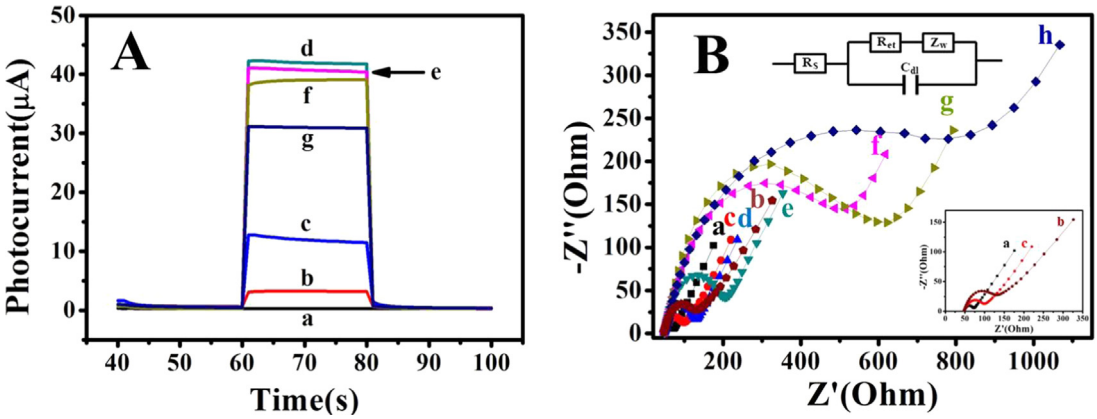

Fig. 3. (A) The photocurrent response of (a) ITO, (b) ITO/Cu_2MoS_4, (c) ITO/G/Cu_2MoS_4, (d) ITO/G/Cu_2MoS_4@CdS:Mn, (e) ITO/G/Cu_2MoS_4@CdS:Mn/Ab, (f) ITO/G/Cu_2MoS_4@CdS:Mn/Ab/BSA and (g) ITO/G/Cu_2MoS_4@CdS:Mn/Ab/BSA/cTnI. (B) The Nyquist diagrams of (a) ITO, (b) ITO/Cu_2MoS_4, (c) ITO/G/Cu_2MoS_4, (d) ITO/G/Cu_2MoS_4/CS, (e) ITO/G/Cu_2MoS_4/CS@CdS:Mn, (f) ITO/G/Cu_2MoS_4/CS@CdS:Mn/Ab, (g) ITO/G/Cu_2MoS_4/CS@CdS:Mn/Ab/BSA and (h) ITO/G/Cu_2MoS_4/CS@CdS:Mn/Ab/BSA/cTnI.

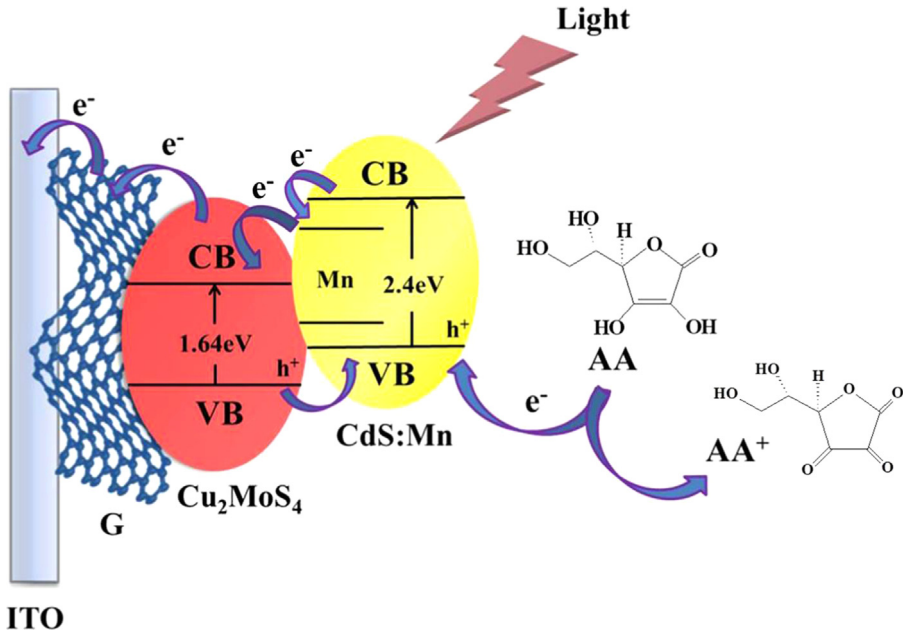

Scheme 2. Schematic diagram of electron-transfer mechanism.

follows: at low concentration, the thickness of Cu_2MoS_4 film enlarged with the increased concentration, resulted in more photoactive materials and light absorption. However, when the concentrations were higher than 3.0 mg/mL, the thicker Cu_2MoS_4 film could augment diffusional resistance for electron motion (Yang et al., 2015). Therefore, we selected 3.0 mg/mL Cu_2MoS_4 suspension as the optimum concentration for the next experiments.

G as a superb conductive material could increase the photocurrent intensity. Fig. S4 B shows that the photocurrent intensity increased accordingly with the G concentration increased from 0.10 mg/mL to 0.25 mg/mL. Nevertheless, when the G concentration increasing to 0.85 mg/mL, the photocurrent intensity gradually decreased, which could attribute to that the excess G caused more resistance rather than conductivity (Tsai et al., 2011). Thus, 0.25 mg/mL G suspension was employed as the first-rank concentration for further experiments.

The coating numbers of CdS:Mn could reflect the thickness of CdS:Mn. The effect of coating numbers was investigated in the range of 1–10 (Fig. S4 C). The photocurrent intensity increased significantly with the increase of coating number, which could be attributed to that the CdS:Mn enlarged light absorption range and accelerated the charge transfer rate. When the coating numbers were 8, the photocurrent intensity was the highest. Therefore, 8 coating numbers of CdS:Mn NPs were chosen as the optimal condition for the subsequent use.

AA was served as an ideal electron donor to capture photogenerated holes to inhibit the recombination of electron-hole pairs (Han et al., 2018; Wang et al., 2017a). The influence of AA concentrations to photocurrent was shown in the Fig. S4 D. The photocurrent intensity increased with the increasing concentration of AA, and got the optimal value at 0.1 mol/L. As the concentration of AA further increased, the photocurrent showed a downward trend because of the quenched absorbance of the electrolyte solution (Wang et al., 2017a), which thus decreased the light intensity and formation efficiency of excited electron-hole center (Kang et al., 2010). Hence, 0.1 mol/L AA was selected as the appropriate concentration of electron donor for these experiments.

Fig. S4 E exhibited the optimizational result of light wavelength response. We investigated the light wavelength response of the synthesized materials in the wavelength range of 365–530 nm because the composites had a strong UV–vis absorption in 300–600 nm (Fig. S5). When under the irradiation of 450 nm light source, the photocurrent intensity had a maximum value (51.57 μA). As a result, 450 nm was chosen as the best illumination for the following use.

3.4. Performance of the PEC immunosensor for the cTnI detection

Under the optimum immunoassay conditions, the different concentrations of cTnI were tested by the as-fabricated PEC immunosensor. Fig. 4 A exhibits the photocurrent responses of different concentrations. The photocurrent gradually decreased as the cTnI concentration increased, meaning more cTnI Ag was hatched on the electrode and involved in the PEC process. It can be seen from Fig. 4 B, with the logarithm of cTnI concentration in the range from 5 pg/mL to 1000 ng/mL, the photocurrent intensity was linearly decreased. The calibration equation was I = -2.60 log$c$ + 31.01 with the correlation coefficients of 0.9946. The detection limit was estimated in line accordance with the signal-to-noise ratio was 3 (S/N = 3) (Li et al., 2016). In this method, the first was to calculate the standard deviation (S.D.) of PEC responses of five replicated measurements of G/Cu_2MoS_4/CS@CdS:Mn/Ab/BSA electrodes. Then the calculated 3 S.D./k as the value of detection limit, in which k was the slope of the linear regression quation of calibration curve. Therefore, the detection limit (3 S/N) was estimated to be 0.18 pg/mL. Compared with other reported works for cTnI detection, our work had a lower detection limit and wider detection range (showed in Table S1), which indicated this immunosensor had high sensitivity and could be used in detecting of cTnI. Meanwhile, compared with other works (Li et al., 2017b; Tan et al., 2017), PEC immunoassay for cTnI detection had fast response, simple operation and a low background signal.

3.5. Stability, selectivity and reproducibility of the PEC immunosensor

For the application, excellent stability, high selectivity and good reproducibility are the important characteristics of the immunosensor (Wu et al., 2018; Xiang et al., 2018a, 2018b). Fig. 4 C shows the recording of the photocurrent response for the detection of 10 ng/mL cTnI under repeated 10 times on-off-on operation. There are no obvious photocurrent changes were observed, indicating the proposed immunosensor had excellent stability for the detection of cTnI.

Selective research of the PEC immunosensor for cTnI detection was carried out with some interfering substance, such as insulin, glucose,

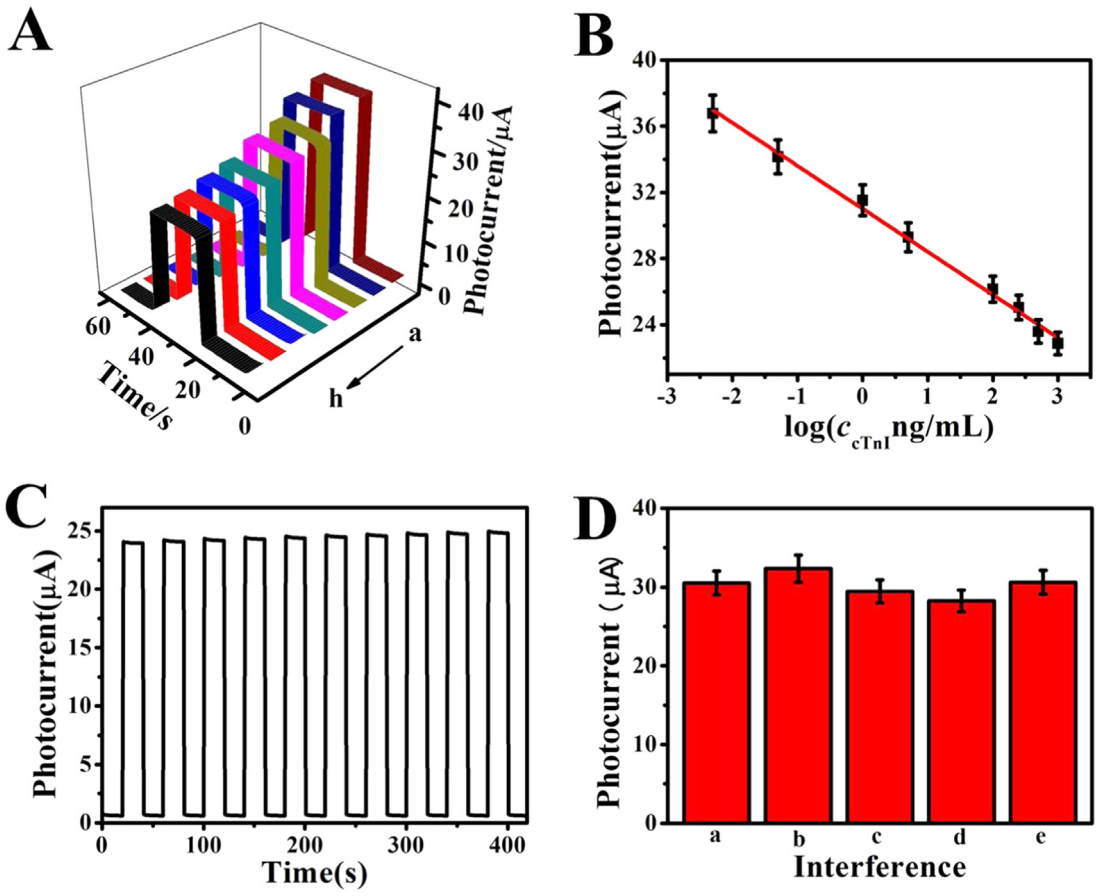

Fig. 4. (A) Photocurrent responses to different concentrations of cTnI solutions: (a - h) 0.005, 0.05, 1, 5, 100, 250, 500, and 1000 ng/mL. (B) The calibration curve of the immunosensor for different concentrations of cTnI. (C) The photocurrent responses of PEC biosensor for the detection of 10 ng/mL cTnI under repeated 10 times on/off irradiation. (D) The PEC photocurrent intensity responses to (a) 10 ng/mL cTnI, (b) 10 ng/mL cTnI + 50 ng/mL insulin, (c) 10 ng/mL cTnI + 50 ng/mL glucose, (d) 10 ng/mL cTnI + 50 ng/mL HIgG and (e) 10 ng/mL cTnI + 50 ng/mL UA.

human immunoglobulin antigen (HIgG) and uric acid (UA). 10 ng/mL of cTnI solution comprising 50 ng/mL interfering substances were tested respectively under the same experimental condition and the tested results were shown in Fig. 4 D. Compared with the result of 10 ng/mL cTnI, there were no distinct change in photocurrent, and the relative standard deviation (RSD) of the measurement was within 5.0%, indicating the selectivity of the immunosensor was acceptable.

Reproducibility of the biosensor was investigated by measuring five fabricated electrodes with 10 ng/mL cTnI under the identical experimental conditions. Fig. S6 shows the photocurrent intensities of five electrodes were similar, and the RSD of measurements was 1.7%, indicating the reproducibility of this immunosensor was satisfactory.

3.6. Real sample analysis

To further research the feasible application of the biosensor for real sample analysis, the different concentrations (20, 40, 60 pg/mL) of cTnI in normal serum samples were measured via standard addition methods. Table S2 exhibits the analytical results, from which we can see the recovery was in the range of 99.3–100.6%, the RSD was in the range of 1.5–2.0%, demonstrating that the fabricated biosensor could be preliminarily applied in clinical diagnosis.

4. Conclusion

In this work, we developed a novel label-free PEC biosensor for the detection of cTnI based on CdS:Mn NPs sensitized G/Cu_2MoS_4 composite. The sheet structure of G/Cu_2MoS_4 provided a large specific surface for the loading of CdS:Mn NPs. What's more, graphene also improved the electron conduction ability of the G/Cu_2MoS_4@CdS:Mn matrix, further enhanced the photocurrent. The CdS:Mn NPs as an outstanding photosensitizer effectively enhanced the PEC performance of the proposed PEC biosensor. Under optimal experimental conditions, the constructed PEC biosensor showed excellent stability, acceptable selectivity and satisfactory reproducibility, with a broad detection range of 0.005–1000 ng/mL and a low detection limit of 0.18 pg/mL. In view of the outstanding merits of designed PEC immunosensor, it may offer a promising method for cTnI detection in clinical diagnosis and also provide a potential application for other disease biomarker detection.

Acknowledgments

We gratefully acknowledge the financial support of the National Natural Science Foundation of China (Grant no. 21775054), the Natural Science Foundation of Shandong Province (Grant no. ZR2016JL013), Postdoctoral Science Foundation of China (Grant no. 2017M622116) and University of Jinan (Grant no. XBH1703). All of the authors express their sincere thanks.

Credit author statement

All persons who meet authorship criteria are listed as authors, and all authors certify that they have participated sufficiently in the work to take public responsibility for the content, including participation in the concept, design, analysis, writing, or revision of the manuscript. Furthermore, each author certifies that this material or similar material

has not been and will not be submitted to or published in any other publication before its appearance in the *Biosensors and Bioelectronics*.

Author contributions

H.T.C. and Q.Z.H. contributed equally to this work. The authors declare no competing financial interest.

Declaration of interests

The authors declare that they have no known competing financial interests or personal relationships that could have appeared to influence the work reported in this paper.

Appendix A. Supplementary material

Supplementary data associated with this article can be found in the online version at doi:10.1016/j.bios.2019.02.048.

References

Adams, J.E., Bodor, G.S., Dávilaromán, V.G., Delmez, J.A., Apple, F.S., Ladenson, J.H., Jaffe, A.S., 1993. Circulation 88, 101–106.
Ahammad, A.J.S., Choi, Y.H., Koh, K., Kim, J.H., Lee, J.J., Lee, M., 2011. Int. J. Electrochem. Sci. 6, 1906–1916.
Asiabanha, R.M., Rasaee, M.J., Mohammadnejad, J., 2016. J. Immunoass. 38, 72–81.
Chekin, F., Vasilescu, A., Jijie, R., Singh, S.K., Kurungot, S., Iancu, M., Badea, G., Boukherroub, R., Szunerits, S., 2018. Sens. Actuators B-Chem. 262, 180–187.
Chen, W., Chen, H., Zhu, H., Gao, Q., Luo, J., Wang, Y., Zhang, S., Zhang, K., Wang, C., Xiong, Y., 2014. Small 10, 4637–4644.
Cummins, B., Auckland, M.L., Cummins, P., 1987. Am. Heart J. 113, 1333–1344.
Cummins, B., Cummins, P., 1987. J. Mol. Cell. Cardiol. 19, 999–1010.
Falahati, A., Sharkey, S.W., Christensen, D., Mccoy, M., Miller, E.A., Murakami, M.A., Apple, F.S., 1999. Am. Heart J. 137, 332–337.
Fan, D., Guo, C., Ma, H., Zhao, D., Li, Y., Wu, D., Wei, Q., 2016. Biosens. Bioelectron. 75, 116–122.
Fan, G.C., Han, L., Zhu, H., Zhang, J.R., Zhu, J.J., 2014a. Anal. Chem. 86, 12398–12405.
Fan, G.C., Ren, X.L., Zhu, C., Zhang, J.R., Zhu, J.J., 2014b. Biosens. Bioelectron. 59, 45–53.
Gopalan, A., Muthuchamy, N., Lee, K., 2016. Biosens. Bioelectron. 89, 352–360.
Haddour, N., Chauvin, J., Gondran, C., Cosnier, S., 2006. J. Am. Chem. Soc. 128, 9693–9698.
Han, J., Liu, Z., Guo, K., Bo, W., Zhang, X., Hong, T., 2015. Appl. Catal. B-Environ. 163, 179–188.
Han, Q., Wang, R., Xing, B., Chi, H., Wu, D., Wei, Q., 2018. Biosens. Bioelectron. 106, 7–13.
Han, Q., Wang, R., Xing, B., Zhang, T., Khan, M.S., Wu, D., Wei, Q., 2017. Biosens. Bioelectron. 99, 493–499.
Kang, Q., Yang, L., Chen, Y., Luo, S., Wen, L., Cai, Q., Yao, S., 2010. Anal. Chem. 82, 9749–9754.
Kim, J.I., Sillah, A., 2013. J. Am. Heart Assoc. 2, e000058.
Kim, K., Park, C., Kwon, D., Kim, D., Meyyappan, M., Jeon, S., Lee, J.S., 2016. Biosens. Bioelectron. 77, 695–701.
Ko, S., Kim, B., Jo, S.S., Oh, S.Y., Park, J.K., 2007. Biosens. Bioelectron. 23, 51–59.
Kucherenko, I.S., Soldatkin, O.O., Lagarde, F., Jaffrezic-Renault, N., Dzyadevych, S.V., Soldatkin, A.P., 2015. Talanta 144, 604–611.
Li, X., Wang, Y., Shi, L., Ma, H., Zhang, Y., Du, B., Wu, D., Wei, Q., 2017a. Biosens. Bioelectron. 96, 113–120.
Li, X., Yu, S., Yan, T., Zhang, Y., Du, B., Wu, D., Wei, Q., 2016. Biosens. Bioelectron. 89, 1020–1025.
Li, X., Zhu, L., Zhou, Y., Yin, H., Ai, S., 2017b. Anal. Chem. 89, 2369–2376.
Lv, S., Zhang, K., Lin, Z., Tang, D., 2017. Biosens. Bioelectron. 96, 317–323.
Ma, N., Wei, B., Cao, W., Gao, H., Xu, L., 2017. Mater. Lett. 197, 79–82.
Masson, J.F., Obando, L., Beaudoin, S., Booksh, K., 2004. Talanta 62. pp. 865–870.
Mcdonnell, B., Hearty, S., Leonard, P., O'Kennedy, R., 2009. Clin. Biochem. 42, 549–561.
Qing, W., Fang, L., Xiaohai, Y., Kemin, W., Hui, W., Xin, D., 2015. Biosens. Bioelectron. 64, 161–164.
Ren, X., Ma, H., Zhang, T., Zhang, Y., Yan, T., Du, B., Wei, Q., 2017a. ACS Appl. Mater. Interfaces 9, 37637–37644.
Ren, X., Yan, J., Wu, D., Wei, Q., Wan, Y., 2017b. ACS Sens. 2, 1267–1271.
Ren, X., Zhang, T., Wu, D., Yan, T., Pang, X., Du, B., Lou, W., Wei, Q., 2017c. Biosens. Bioelectron. 94, 694–700.
Sankapal, B.R., Mane, R.S., Lokhande, C.D., 2000. Mater. Res. Bull. 35, 177–184.
Santra, P.K., Kamat, P.V., 2012. J. Am. Chem. Soc. 134, 2508–2511.
Shen, W., Tian, D., Cui, H., Yang, D., Bian, Z., 2011. Biosens. Bioelectron. 27, 18–24.
Shumkov, A.A., Suprun, E.V., Shatinina, S.Z., Lisitsa, A.V., Shumyantseva, V.V., 2013. Bionanoscience 3, 216–222.
Si, Y.H., Xia, Y., Shang, S.K., Xiong, X.B., Zeng, X.R., Zhou, J., Li, Y.Y., 2018. Nanomaterials 8, 526–537.
Sun, B., Qiao, F., Chen, L., Zhao, Z., Yin, H., Ai, S., 2014. Biosens. Bioelectron. 54, 237–243.
Tan, Y., Wang, Y., Li, M., Ye, X., Wu, T., Li, C., 2017. Biosens. Bioelectron. 91, 741–746.
Tong, Z., Xing, B., Han, Q., Lei, Y., Dan, W., Xiang, R., Qin, W., 2018. Anal. Chim. Acta 1032, 114–121.
Tsai, T.H., Chiou, S.C., Chen, S.M., 2011. Int. J. Electrochem. Sci. 6, 3333–3343.
Wang, G.L., Xu, J.J., Chen, H.Y., Fu, S.Z., 2009a. Biosens. Bioelectron. 25, 791–796.
Wang, G.L., Yu, P.P., Xu, J.J., Chen, H.Y., 2009b. J. Phys. Chem. C 113, 11142–11148.
Wang, X., Xu, R., Sun, X., Wang, Y., Ren, X., Du, B., Wu, D., Wei, Q., 2017a. Biosens. Bioelectron. 96, 239–245.
Wang, Y., Chen, F., Ye, X., Wu, T., Wu, K., Li, C., 2017b. Sens. Actuators B-Chem. 245, 205–212.
Wang, Y., Ge, S., Zhang, L., Yu, J., Yan, M., Huang, J., 2016. Biosens. Bioelectron. 89, 859–865.
Wu, D., Liu, Y., Wang, Y., Hu, L., Ma, H., Wang, G., Wei, Q., 2016. Sci. Rep. 6, 20511–20517.
Wu, D., Wei, Y., Ren, X., Ji, X., Liu, Y., Guo, X., Liu, Z., Asiri, A.M., Wei, Q., Sun, X., 2018. Adv. Mater. 30, 1705366–1705372.
Wu, Q., Sun, Y., Zhang, D., Li, S., Zhang, Y., Ma, P., Yu, Y., Wang, X., Song, D., 2017. Biosens. Bioelectron. 96, 288–293.
Xiang, R., Dan, W., Ge, R., Xu, S., Ma, H., Tao, Y., Yong, Z., Du, B., Qin, W., Liang, C., 2018a. Nano Res. 11, 2024–2033.
Xiang, R., Peng, L., Rui, F., Tong, Z., Yong, Z., Dan, W., Qin, W., 2018b. Talanta 188, 593–599.
Xing, B., Zhu, W., Zheng, X., Zhu, Y., Qin, W., Dan, W., 2018. Sens. Actuators B-Chem. 265, 403–411.
Yan, W.Y., Zhou, Q., Chen, X., Yang, Y., Zhang, Y., Huang, X.J., Wu, Y.C., 2016. J. Hazard. Mater. 314, 41–50.
Yang, J., Gao, P., Liu, Y., Li, R., Ma, H., Du, B., Wei, Q., 2015. Biosens. Bioelectron. 64, 13–18.
Zhan, F., Jie, L., Li, W., Yang, Y., Liu, W., Li, Y., 2016. J. Power Sources 325, 591–597.
Zhang, K., Lv, S., Lin, Z., Tang, D., 2017a. Biosens. Bioelectron. 95, 34–40.
Zhang, T., Ma, N., Ali, A., Wei, Q., Wu, D., Ren, X., 2018. Biosens. Bioelectron. 119, 176–181.
Zhang, Y., Liu, Y., Li, R., Khan, M.S., Gao, P., Yong, Z., Qin, W., 2017b. Sci. Rep. 7, 4629–4636.
Zhao, W.W., Xu, J.J., Chen, H.Y., 2017. Anal. Chem. 90, 615–627.
Zhou, W., Li, K., Wei, Y., Hao, P., Chi, M., Liu, Y., Wu, Y., 2018. Biosens. Bioelectron. 106, 99–104.